Catalysis Science & Technology

Accepted Manuscript

ROYAL SOCIETY OF CHEMISTRY

www.rsc.org/catalysis

Cite this: DOI: 10.1039/c0xx00000x

www.rsc.org/xxxxxx

ARTICLE TYPE

Post-synthesis incorporation of Al into germanosilicate ITH zeolite: the influence of treatment conditions on acidic properties and catalytic behavior in tetrahydropyranylation reaction

Mariya V. Shamzhy,[a,b] Maksym V. Opanasenko,[a,b] Francisca S. de O. Ramos,[a,c] Libor Brabec,[a] Michal Horáček,[a] Marta Navaro-Rojas,[d] Russell E. Morris,[d] Heloise de O. Pastore,[c] and Jiří Čejka*[a]

Received (in XXX, XXX) Xth XXXXXXXXX 20XX, Accepted Xth XXXXXXXXX 20XX
DOI: 10.1039/b000000x

Post-synthesis alumination of germanosilicate medium-pore **ITH** zeolite was shown to be an effective procedure for tuning its acidity. The treatment of **ITH** zeolites synthesized with different chemical compositions (i.e. Si/Ge = 2.5; 4.4; 5.8) with $Al(NO_3)_3$ aqueous solution led to the formation of strong Brønsted and Lewis acid sites and an increasing fraction of ultramicro- and mesopores in Ge-rich **ITH** samples (Si/Ge = 2.5 and 4.4). The concentration of Al incorporated in the framework increases with decreasing Si/Ge ratio in the parent **ITH**. The increasing temperature of alumination from 80 to 175 °C (HT conditions) resulted in 1) 1.5 – 2-fold increase in the concentration of Brønsted acid sites formed; and 2) in decreasing fraction of framework Al atoms detectable with base probe molecules (i.e. pyridine, 2,6-di-*tert*-butyl-pyridine), i.e. an increased concentration of the "inner" acid sites. The activity of prepared Al-substituted **ITH** zeolites in tetrahydropyranylation of alcohols is enhanced with increasing amount of accessible acid sites in bulky crystals (e.g. alumination at lower temperature) or with growth the total concentration of acid centres within tiny **ITH** crystals (e.g. alumination under HT conditions). This trend became more prominent with increasing kinetic diameter of substrate molecules under investigation (methanol < 1-propanol < 1-hexanol).

1. Introduction

The role of zeolites in the current petroleum-based industry can hardly be overestimated. Aluminosilicate zeolites possessing strong acid centres have been widely used as heterogeneous catalysts for a great variety of processes.[1] The applications of medium-pore zeolites as industrial catalysts and the recognition of the *'shape selective'* properties of these materials[2] has stimulated a synthetic work aimed at preparing new microporous materials with various pore sizes and structures.[3-8]

Zeolite **ITH,** possessing three sets of interconnecting medium-pore 9- (4.0 x 4.9 Å), 10- (4.8 x 5.7 Å) and 10- (4.7 x 5.1 Å) ring channels, was first synthesized as a pure silicate in concentrated reaction mixtures (H_2O / T^{IV} < 10, where T is the zeolite framework tetrahedral atom) using hexamethonium as structure-directing agent (SDA).[9] Introducing Al during the synthesis was reported to diminish the crystallization rate of **ITH** while favouring the formation of EU-1 phase.[10] On the other hand, the smaller B–O–Si angles were claimed to facilitate the introduction of B into **ITH** framework with respect to the EU-1 structure, although in relatively small amounts (Si/B ratios >50).[10] Similarly, Al present in the initial gel was also reported that limited the crystallization field of germanosilicate **UTL** zeolite in favour of **STF** phase,[11] while B influences the selectivity of **UTL** zeolite formation to a lesser extent.[12] Attempts to generate strong acid centres by post-synthesis alumination of borosilicate **ITH** zeolite resulted in exchange of only a fraction of boron atoms yielding **ITH** with Si/Al molar ratio of 80 (45 and 105 μmol g^{-1} of Brønsted and Lewis acid sites, respectively).[13] At the same time, Al-containing **ITH** zeolite with an increased concentration of Brønsted acid sites (63 and 48 μmol g^{-1} of Brønsted and Lewis acid sites, respectively) was synthesized directly only in the presence of Ge exploiting its propensity to increase the nucleation rate of zeolites containing D4R SBUs (e.g., **ITH**).[13] Al-**ITH** was shown as shape selective catalyst for conversion of aromatics[14] and catalytic cracking of vacuum gasoil producing propylene.[13]

Pure germanosilicate **ITH** zeolites characterized by Si/Ge ratios in the range 6 – ∞ were prepared using hexamethonium as SDA.[15] Ge was found to preferentially occupy T-sites in the D4Rs.[15] Recently, Ren *et al.* reported the synthesis of Ge-enriched **ITH** zeolites (2 < Si/Ge < 6) in a dilute medium (H_2O / T^{IV} = 22 – 66) using N,N,N',N'-tetramethyl-1,6-hexanediamine (TMHDA) as template.[16]

The possibility to tune the strength of acid centres by post-synthesis substitution of Al and Ga for B and Ge in the framework of borogermanosilicate large-pore **IWR** zeolite was shown and confirmed by means of X-ray powder diffraction, chemical analysis and infrared spectroscopy of adsorbed

pyridine.[17] The catalytic performance of prepared isomorphously substituted **IWR** zeolites in Friedel-Crafts acylation reaction was also evaluated.[17]

In this paper, we successfully extended this approach to generate strong acid centres by post-synthesis alumination of medium-pore germanosilicate **ITH** zeolites. The formation of ultramicropores and mesopores at the expense of Ge extraction was observed when using Ge-rich **ITH** zeolites with Si/Ge = 2.5 or 4.4 as starting materials. It will be shown that the temperature of post-synthesis treatment strongly influences the concentration of Brønsted acid sites formed and their accessibility. The improved catalytic behaviour of aluminated **ITH** zeolites containing strong acid centres with respect to initial germanosilicates was demonstrated in tetrahydropyranylation reaction (**Scheme** 1) commonly used for protection of hydroxyl groups in peptide, nucleotide, carbohydrate, and steroid chemistry.[18]

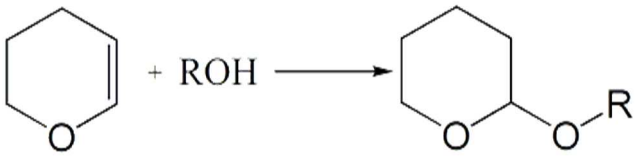

Scheme 1 Tetrahydropyranylation of alcohols

2. Experimental part

2.1 Materials

1,6-Dibromohexane (96%), trimethylamine solution (31 – 35 wt.% in ethanol), N,N,N',N'-tetramethyl-1,6-hexanediamine (99%), germanium oxide (99.99%), tetraethylorthosilicate (TEOS, 98%), aluminium nitrate nonahydrate (≥98.5%) were used for the synthesis and post-synthesis treatment of zeolites. 3,4-Dihydro-2*H*-pyran (DHP, 97%), methanol (≥99.9%), 1-propanol (≥99.9%), 1-hexanol (≥99.5%), mesitylene (≥99%) and hexane (≥97%) were used in catalytic experiments. All reactants and solvents were obtained from Sigma Aldrich and used as received without any further treatment.

2.2 Preparation of hexamethonium dihydroxide

Hexamethylene-bis(trimethylammonium)dibromide was prepared according to the Ref.[19] and transformed into hydroxide form using Bio-Rad AG-1X8 anion exchange resin. The solution of hexamethonium dihydroxide was concentrated (evaporated at p = 25 Torr, T = 35 °C) until the hydroxide concentration became 1.0 mol L^{-1}.

2.3 Synthesis of ITH zeolites

The zeolites prepared in his study were designated as *ITH-n*, where "n" is Si/Ge in the reaction mixture.

Ge-poor zeolite *ITH-6* was synthesized according to Ref.[10] using hexamethonium dihydroxide as SDA. The starting gel had the following composition: 0.86 SiO_2 : 0.14 GeO_2 : 0.25 $SDA(OH)_2$: 5 H_2O. Typically, a certain amount of germanium oxide (GeO_2) was dissolved in a solution of $SDA(OH)_2$ (1.0 mol L^{-1}). Then, TEOS was added and the mixture was gently stirred at room temperature until complete evaporation of the alcohol formed. The resulting fluid gel was charged into 25 ml Teflon-lined autoclave and heated at 175 °C for 20 days under agitation (~ 60 rpm). The solid product was separated by filtration, washed with distilled water and dried overnight at 65 °C. The occluded hexamethonium was removed from the samples by heating the products from room temperature to 300 °C at a rate of 1 °C min^{-1}, and kept at that temperature for 3 h. The next step involved increasing the temperature at a rate of 1 °C min^{-1} up to 580 °C; the temperature was maintained under air flow (200 mL min^{-1}) for 3 h, to remove the remaining organic.

Ge-rich zeolites *ITH-1* and *ITH-2* were prepared according to the Ref.[16] N,N,N',N'-tetramethyl-1,6-hexanediamine (TMHDA) was used as the structure directing agent. The synthetic suspension had the composition of (1-x) SiO_2: x GeO_2: 7 TMHDA: 1.4 HF: 44 H_2O, where x = 0.5 for *ITH-1* and x = 0.33 for *ITH-2*. The reaction mixture was heated at 175 °C for 6 days under static condition.

The as-synthesized samples *ITH-1* and *ITH-2* were washed with distilled water, dried at 65 °C for 12 h and calcined at 650 °C for 8 h with a temperature ramp of 1 °C·min^{-1} under air flow (200 mL min^{-1}).

2.4 Post-synthesis treatment

Post-synthesis alumination of **ITH** zeolites was performed by

- stirring of the parent **ITH** zeolite in 1 mol L^{-1} solution of $Al(NO_3)_3$ (1g zeolite/100 ml solution) at T = 80 °C, pH = 2.0 for 96 h;
- treatment of the parent **ITH** zeolite in 1 mol L^{-1} solution of $Al(NO_3)_3$ (1g zeolite/100 ml solution) at T = 175 °C, pH = 2.0 for 24 h in autoclave.

The solid product was centrifuged and extensively washed with distilled water until the filtrate was neutral and then dried overnight at room temperature.

The prepared samples are designated in the following way: *ITH-n /Al/ temperature (°C)*.

2.5 Characterization

The crystallinity of all samples under investigation were determined by X-ray powder diffraction (XRD) using a Bruker AXS-D8 Advance diffractometer with a graphite monochromator and a position sensitive detector (Våntec-1) using CuKα radiation in Bragg–Brentano geometry at a scan rate of 0.25° 2θ min^{-1}.

Nitrogen adsorption/desorption isotherms were measured using an ASAP 2020 (Micromeritics) static volumetric apparatus at liquid nitrogen temperature (–196 °C). Prior to the sorption measurements, all samples were degassed with a turbomolecular pump at 300 °C for 8 h.

The size and shape of zeolite crystals were examined by scanning electron microscopy (SEM, JEOL JSM-5500LV microscope). For the measurement the crystals were coated with a thin layer of platinum (~ 10 nm) in a BAL-TEC SCD-050 instrument.

The concentration of Al, Ge and Si in zeolites was determined by energy dispersive X-ray spectroscopy (EDX) using a Jeol JSM 5600 instrument.

Solid-state ^{27}Al NMR spectra were obtained using a Bruker Advance III spectrometer, equipped with a 9.4 T wide-bore superconducting magnet (^{1}H Larmor frequency of 400.13 MHz). The samples were packed into conventional 4 mm zirconia rotor,

Cite this: DOI: 10.1039/c0xx00000x

www.rsc.org/xxxxxx

ARTICLE TYPE

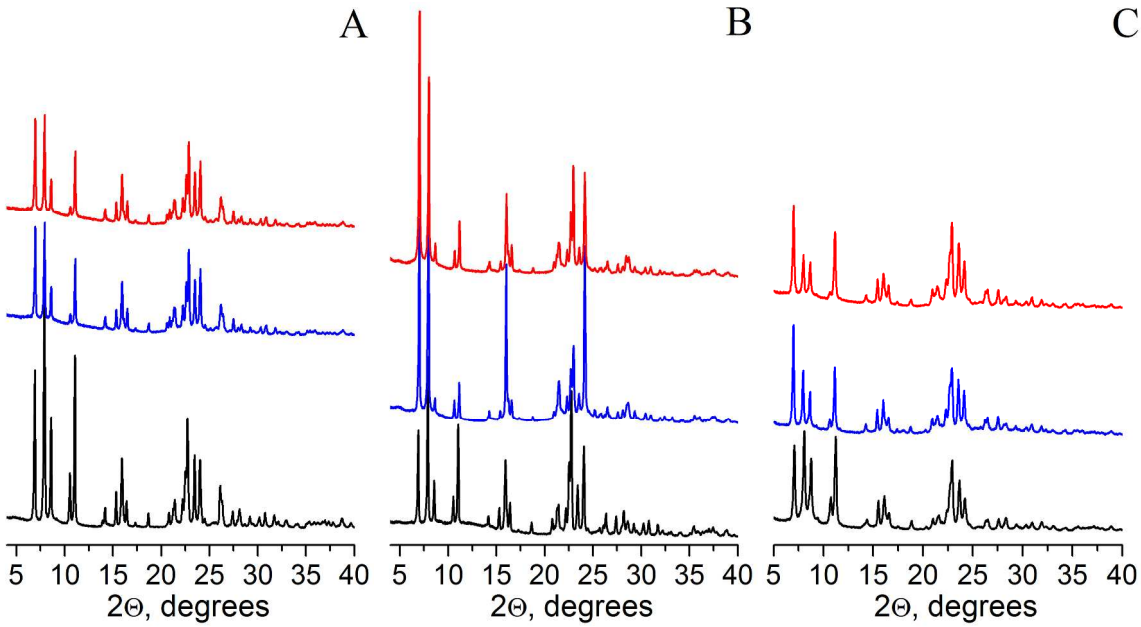

Fig. 1 XRD patterns of *ITH-1* (**A**), *ITH-2* (**B**), *ITH-6* (**C**) zeolites: initial germanosilicates (black), *ITH-n/Al/80* (blue) and *ITH-n/Al/175* (red)

and rotated at a MAS rate of 12.5 kHz using a Bruker 4 mm HFXY probe. A pulse of 1.5 μs ($\nu_1 \approx 100$ kHz) was applied. Signal averaging was carried out for 200 transients with a repeat interval of 2 s. Spectra were referenced to 1.1 M $Al(NO_3)_3$ in D_2O using solid $Al(acac)_3$ ($\delta_{iso} = 0$ ppm, centre of gravity = –4.2 ppm at 9.4 T) as a secondary reference.

The concentration of Lewis (c_L) and Brønsted (c_B) acid sites was determined after adsorption of pyridine (Py) by FTIR spectroscopy using a Nicolet Protégé 460 Magna with a transmission MTC/A detector. The zeolites were pressed into self-supporting wafers with a density of 8.0 – 12 mg cm^{-2} and activated in situ at T = 450 °C and p = $5 \cdot 10^{-5}$ Torr for 4 h. Pyridine adsorption was carried out at 150 °C for 20 min at a partial pressure of 3.5 Torr, followed by desorption for 20 min at the same temperature. Before adsorption pyridine was degassed by freezing-pump-thaw cycles. All spectra were recorded with a resolution of 4 cm^{-1} by collecting 128 scans for a single spectrum at room temperature. Spectra were recalculated using a wafer density of 10 mg cm^{-2}. Concentration of c_L and c_B were evaluated from the integral intensities of bands at 1454 cm^{-1} (c_L) and at 1545 cm^{-1} (c_B) using extinction coefficients, ε(L) = 2.22 cm μmol^{-1}, and ε(B) = 1.67 cm μmol^{-1} [20].

A relatively large probe molecule 2,6-di-*tert*-butyl-pyridine (DTBP) was used to determine the accessibility of acid sites in the prepared zeolites.[21] The adsorption of DTBP took place at 150 °C for 15 min at an equilibrium vapour pressure of the probe molecule. Desorption proceeded at the same temperature for 1 h followed by collection of spectra at room temperature. Extinction coefficients determined in Ref.[20] were used for the evaluation of c_B adsorbing DTBP.

2.6 Tetrahydropyranylation of alcohols

The catalytic experiments were performed in the liquid phase under atmospheric pressure at room temperature (25 °C) in a multi-experiment workstation Star-Fish (Radleys Discovery Technologies). Before use, the catalyst (100 mg) was activated at 450 °C for 90 min at a rate of 10 °C min^{-1}. Typically, alcohol (i.e. methanol, 1-propanol or 1-hexanol, 9 mmol), mesitylene (0.4 g; internal standard), hexane (10 ml, solvent) and the catalyst (100 mg) were added to a two-necked vessel equipped with a thermometer. DHP (15 mmol) was then added to the vessel. Samples of the reaction mixture were taken periodically and analyzed by using Agilent 6850 GC equipped a nonpolar DB-5 column (length 20 m, diameter 0.180 mm, and film thickness 0.18 mm) and a flame ionization detector.

The reaction products were identified by using Thermo Finnigan Focus DSQ II Single Quadrupole GC/MS.

3. Results and discussion

The X-ray diffraction patterns of germanosilicate **ITH** zeolites (**Fig. 1**) used as starting materials for alumination match well with those reported in the literature.[22] In contrast to *ITH-1* and *ITH-2* possessing platelet-like crystals, *ITH-6* is characterized by needle-like crystals (**Fig. 2**). While samples *ITH-1* and *ITH-2* present separated crystals of remarkably higher size (**Fig. 2A, D**, **Table 1**), the Ge-poor *ITH-6* sample shows the agglomerates of

Cite this: DOI: 10.1039/c0xx00000x

www.rsc.org/xxxxxx

ARTICLE TYPE

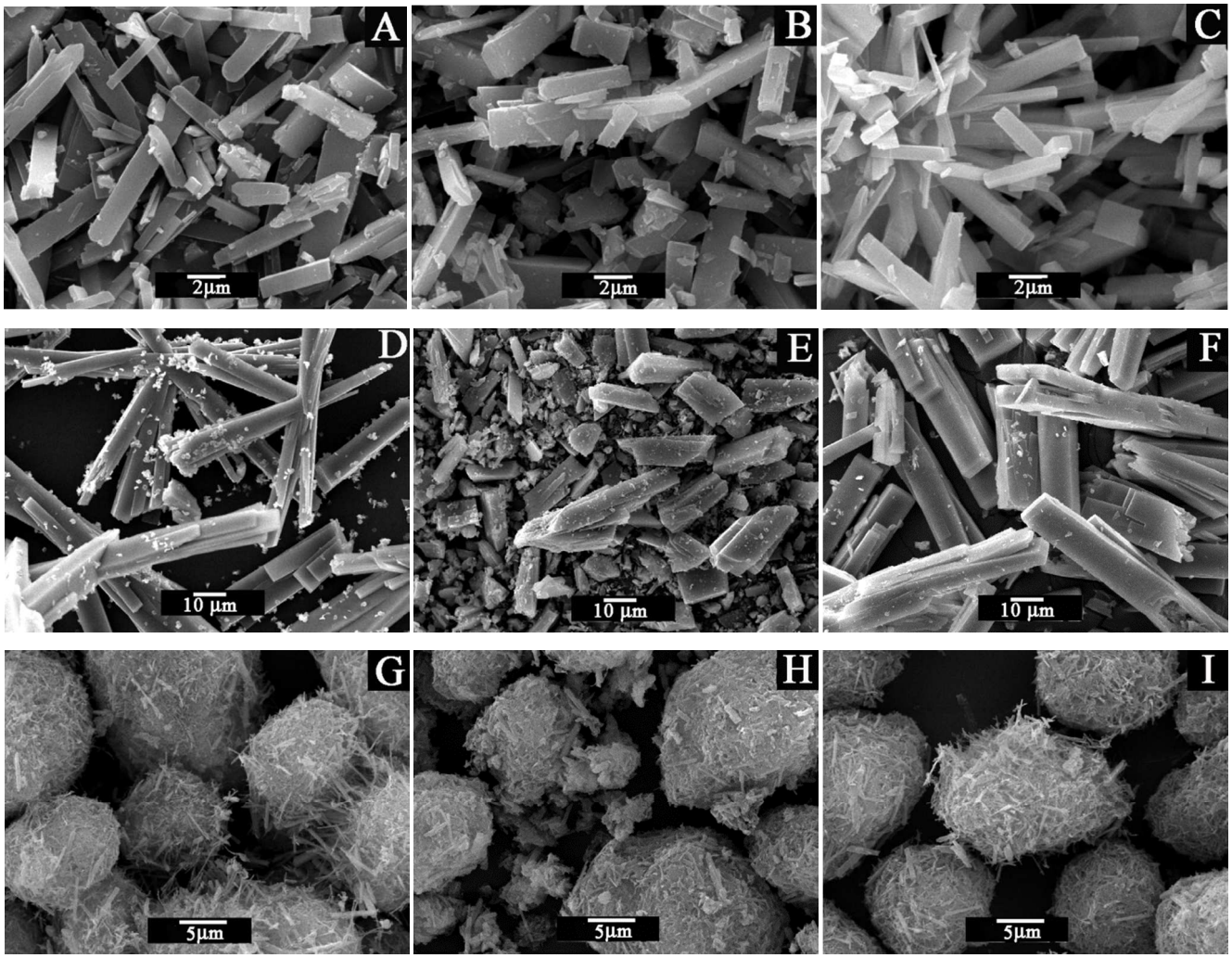

Fig. 2 SEM images of **ITH** zeolites under investigation : *ITH-1* (**A**); *ITH-1/Al/80* (**B**); *ITH-1/Al/175* (**C**); *ITH-2* (**D**); *ITH-2/Al/80* (**E**); *ITH-2/Al/175* (**F**); *ITH-6* (**G**); *ITH-6/Al/80* (**H**); *ITH-6/Al/175* (**I**)

tiny crystals (**Fig. 2G**, **Table 1**). This result may be connected with a higher rate of crystal growth in the presence of TMHDA acting as SDA for *ITH-1* and *ITH-2* samples. The broader and less intense diffraction lines characteristic for *ITH-6* zeolite in comparison with *ITH-1* and *ITH-2* samples (**Fig. 1**) are consistent with smaller size of *ITH-6* crystals (**Fig. 2**). *ITH-1* and *ITH-2* zeolites exhibit type I isotherm (**Fig. 3 A, B**) characteristic for microporous solids and are characterized by micropore volume of 0.112 and 0.125 cm^3 g^{-1}, respectively (**Table 1**). *ITH-6* germanosilicate representing quite small crystals (ca. 5.0 x 0.5 x 0.5 µm) showed uptake in the range of p/p_s= 0.8 – 1.0 (**Fig. 3C**) most probably attributed to filling of intercrystalline space.

Chemical analysis of the **ITH** zeolites agrees with the composition of corresponding gels showing increasing Si/Ge ratio in the solids with decreasing Ge concentration in reaction mixture (**Table 1**). However, while chemical composition of Ge-poor *ITH-6* zeolite (Si/Ge = 5.8) corresponds to Si/Ge in initial gel, Ge-rich *ITH-1* (Si/Ge = 2.5) and *ITH-2* (Si/Ge = 4.4) samples are characterized by ca. twice lower Si/Ge ratios than those in reaction mixture (**Table 1**). This corresponds to results obtained in Ref.[15, 16] and may be related with "saturation" of T-sites in D4Rs and $[4^1 5^2 6^2]$ cages.

It should be noted that Ge preferentially occupies positions in D4Rs forming [4Si;4Ge] domains regularly located in-between

Cite this: DOI: 10.1039/c0xx00000x

www.rsc.org/xxxxxx

ARTICLE TYPE

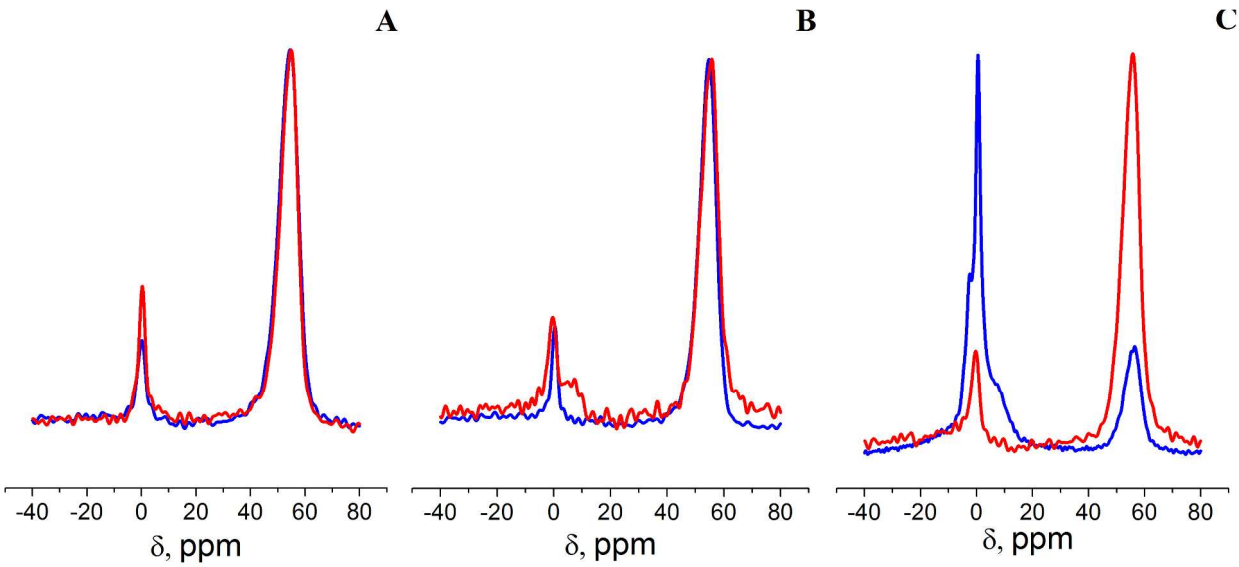

Fig. 3 ^{27}Al MAS NMR spectra of *ITH-1* (A), *ITH-2* (B), *ITH-6* (C) zeolites: *ITH-n/Al/80* (blue) and *ITH-n/Al/175* (red)

silica layers in *ITH-1* and *ITH-2*, while both pure silica [8Si] and Si-rich D4Rs[7Si;1Ge] were detected in Ge-poor (Si/Ge > 5) **ITH** zeolites.[23]

Table 1 Chemical composition and textural characteristics of germanosilicate **ITH** zeolites under investigation

Sample	Chemical composition of zeolites, mol. %		Si/Ge		Crystal size (μm)
	Si	Ge	Reaction mixture	Zeolite	
ITH-1	71.4	28.6	1	2.5	10.0 x 2.5 x 1.0
ITH-2	81.5	18.5	2	4.4	40.0 x 5.0 x 5.0
ITH-6	85.6	14.5	6	5.8	5.0 x 0.5 x 0.5

3.1 The structure and textural properties of post-synthetically treated ITH zeolites

As it was shown in Ref.[23], the acidic treatment of **ITH** zeolites having appropriate amount of Ge in D4R SBUs (i.e. $Si/Ge_{D4R} \leq 1$ like in *ITH-1* sample) results in zeolite disassembly, e.g. the formation of layered material possessing the same topology of the layers as initial **ITH** zeolite. In contrast, all **ITH** zeolites subjected to alumination in acidic medium (pH = 2.0) at T = 80 °C or 175 °C still display sharp diffraction lines at the characteristic 2-theta positions, which proves the preservation of the structure ordering of the samples (**Fig. 1**). This indicates that Al acts as "stabilizer" preventing the disassembly of Ge-rich **ITH** zeolite (i.e. *ITH-1*) in acidic medium. Mentioned effect was also observed for **IWR** zeolite in Ref.[17] and may be connected with rapid healing of defects formed in the course of hydrolysis of Ge-O-Si bonds with Al. No diffraction lines of $Al(NO_3)_3$ or other crystalline admixtures were observed in XRD patterns of **ITH** zeolites after alumination procedures described in this study. The decrease in the intensity of diffraction lines for **ITH** zeolites subjected to alumination, which is especially pronounced for Ge-rich *ITH-1* sample (**Fig. 1A**), likely originates from diminishing of the framework density caused by the leaching of the framework Ge atoms under conditions used (**Table 2**). The aluminated samples showed drastically higher Si/Ge ratio (12.6 – 158) if compared with parent **ITH** zeolites (Si/Ge = 2.5 –5.8). The magnitude of Ge extraction depends both on the temperature of the treatment and the size of zeolite crystals. While *ITH-2/Al/80* and *ITH-2/Al/175* characterized by the bulkiest crystals (40.0 x 5.0 x 5.0 μm, **Table 1**) show close Si/Ge ratios (**Table 2**), higher drop in Ge concentration at 175 vs. 80 °C was observed for *ITH-1* (10.0 x 2.5 x 1.0 μm) and especially *ITH-6* zeolites (5.0 x 0.5 x 0.5 μm).

Table 2 Chemical composition of ITH zeolites subjected to alumination

Sample	Chemical composition, mol.%			Si/Ge	Al_{Th}[a], mol. %
	Al	Ge	Si		
ITH-1	–	28.6	71.4	2.5	–
ITH-1/Al/80	2.6	6.8	90.6	13.3	92
ITH-1/Al/175	4.3	2.2	93.5	42.5	88
ITH-2	–	18.5	81.5	4.4	–
ITH-2/Al/80	1.5	7.0	91.5	13.0	91
ITH-2/Al/175	2.1	7.2	90.7	12.6	84
ITH-6	–	14.5	85.6	5.8	–
ITH-6/Al/80	6.7	4.3	89.0	21.0	24
ITH-6/Al/175	4.0	0.6	95.0	158	89

[a]calculated based on the integral intensities of peaks at 0 and 60 ppm in ^{27}Al NMR spectra

Cite this: DOI: 10.1039/c0xx00000x

www.rsc.org/xxxxxx

ARTICLE TYPE

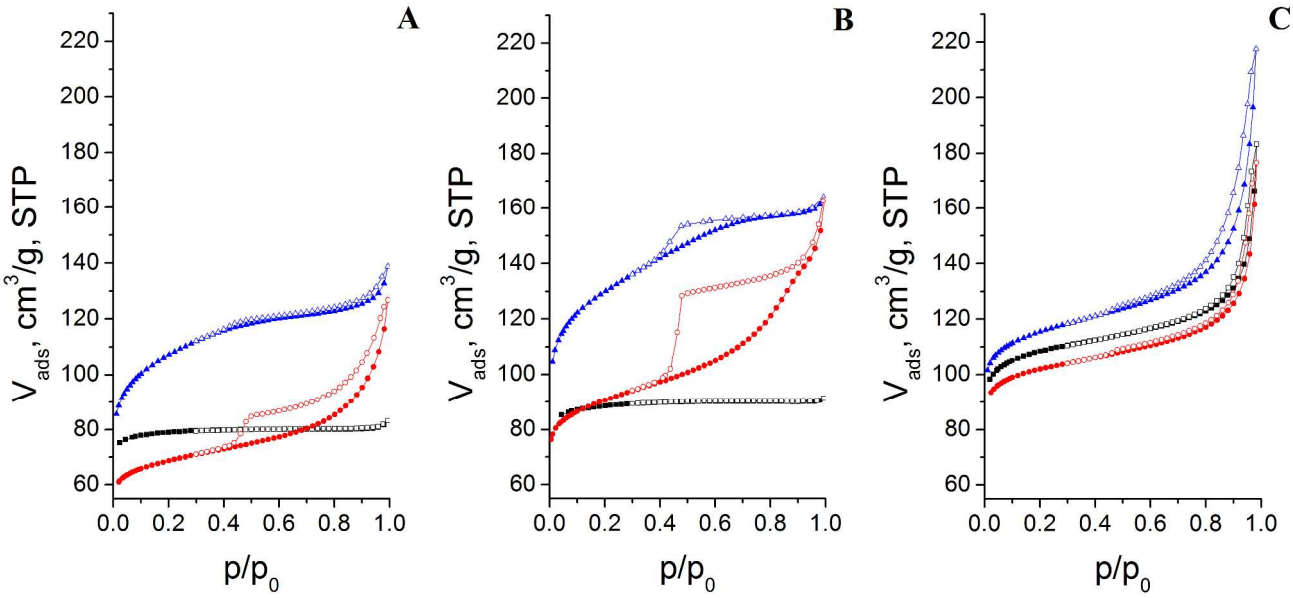

Fig. 4 Nitrogen adsorption (•) and desorption (○) isotherms of *ITH-1* (**A**), *ITH-2* (**B**), *ITH-6* (**C**) zeolites: initial germanosilicates (black), *ITH-n/Al/80* (blue) and *ITH-n/Al/175* (red)

This result indicates the role of diffusion in the degermanation process and is in agreement with previous observations on the influence of zeolite crystal size on dealumination[24] and desilication[25] outcome.

While the results of the chemical analysis indicate increasing concentration of Al (**Table 2**), the solid-state ^{27}Al MAS NMR spectra of all aluminated samples (**Fig. 3**) show the presence of both tetrahedral AlO_4 (shift ranges of 50 – 80 ppm) and octahedral AlO_6 species (-10 – 15 ppm).[26] Ge-rich *ITH-1* and *ITH-2* zeolites aluminated at 80 or 175 °C and *ITH-6/Al/175* sample show a dominant peak at – 54 ppm (~90% of the integrated signal intensity) evidencing the incorporation of the most aluminium atoms into the framework of zeolite (**Fig. 3**). In contrast, the *ITH-6/Al/80* showed the dominant reflex at 0 ppm (76% of the integrated intensity, **Table 2**) attributed to AlO_6 species. It seems, that the output of alumination is dependent on the rates of 3 processes, i.e. 1) extraction of Ge leading to the formation of silanol defects (*vide infra*); 2) healing of formed defects with Al leading to the formation of Brønsted acid sites; and 3) precipitation of oxo-Al species in the internal/intercrystalline voids resulted in a deposition of extra-framework species. The total amount of Al as well as the ratio between framework and extra-framework Al species (**Table 2**) depends both on the treatment condition and intrinsic properties of initial germanosilicate (i.e. crystal size, Si/Ge ratio). Increasing the temperature of the treatment results in the growth of the concentration of Al, incorporated into the framework of *ITH-1* and *ITH-6* zeolites. In contrast, the concentration of Al in *ITH-2* zeolites possessing the bulkiest crystals does not depend significantly on the temperature of the treatment. This result is likely connected either with diffusional restrictions for Ge extraction/Al penetration into bulky crystals. On the other hand, the contamination of extra-framework Al species is favourable for *ITH-6* zeolites possessing tiny crystals when being aluminated at 80 °C (**Table 2**).

The shape of **ITH** platelet-like crystals remained intact during alumination (**Fig. 2**), *ITH-1/Al/80* (**Fig. 2B**) and *ITH-2/Al/80* (**Fig. 2E**) showed increased fraction of cracked tiny crystals (1 – 3 μm) in comparison with the parent *ITH-1* (**Fig. 2A**) and *ITH-2* (**Fig. 2D**) zeolites. In contrast, *ITH-1/Al/175* (**Fig. 2C**) and *ITH-2/Al/175* (**Fig. 2F**) zeolites treated under hydrothermal conditions showed crystals of uniform size close to the parent germanosilicates. This result is probably connected with acceleration of the dissolution/precipitation processes at elevated temperature via Ostwald ripening of **ITH** crystals under hydrothermal conditions. It seems that alumination at higher temperature resulted in an accelerated and more complete recrystallization of *ITH-n* zeolites, while the low temperature treatment led to deterioration of the crystal morphology (destruction or conglutination, **Fig. 2**).

Nitrogen isotherms provide valuable information on the textural properties of aluminated **ITH** zeolites when compared with the parent ones. In contrast to parent germanosilicate *ITH-1* and *ITH-2* zeolites (**Fig.4A, B**) exhibiting type I isotherm, zeolites *ITH-1/Al/80* and *ITH-2/Al/80* aluminated at 80 °C show isotherms of type I with hysteresis loop of H4 characteristic of

Cite this: DOI: 10.1039/c0xx00000x

www.rsc.org/xxxxxx

ARTICLE TYPE

microporous solids with a broad pore size distribution. The magnification of the average pore size in *ITH-1* and *ITH-2* zeolites treated with $Al(NO_3)_3$ solution in acidic medium is most probably connected with breaking of hydrolytically unstable Ge–O(Si) bonds resulting in the increasing void volume. A similar process of mesopores formation in the course of the treatment of germanosilicate **IWW** zeolite with hydrochloric acid at elevated temperature was also observed in Ref. [27] The increase in the alumination temperature leads to the increased fraction of mesopores in *ITH-1/Al/175* and *ITH-2/Al/175* both exhibiting combined type I and type IV isotherms, being typical for hierarchical micro/mesoporous materials. It should be noted, that a contribution of Si extraction in the formation of mesopores at 175 °C cannot be excluded, since *ITH-2/Al/80* and *ITH-2/Al/175* characterized by close Si/Ge ratio (**Table 2**) showed drastically different nitrogen ad-/desorption isotherms (**Fig. 4**). In contrast, alumination does not significantly impact the pore system of Ge-poor *ITH-6* zeolite. Both aluminated *ITH-6/Al/80* and *ITH-6/Al/175* zeolites or parent *ITH-6* germanosilicate possessed similar adsorption/desorption isotherms of type I showing an interparticle adsorption in the range of p/p_0= 0.8 – 1.0 (**Fig. 4C).** The formation of extra-porosity not observing during the alumination of Ge-poor *ITH-6* zeolite treatment with $Al(NO_3)_3$ solution is likely caused by "unsuitable" distribution of extractable Ge atoms in the framework (the absence of [4Si;4Ge] domains according to the NMR data [23]).

Table 3 Textural characteristics of **ITH** zeolites subjected to alumination

Sample	V_{micro} [a], $cm^3 \cdot g^{-1}$	V_{meso} [b], $cm^3 \cdot g^{-1}$	S_{BET} [c], $m^2 \cdot g^{-1}$	S_{ext} [a], $m^2 \cdot g^{-1}$
ITH-1	0.112	0.007	285	23
ITH-1/Al/80	0.103	0.05	330	143
ITH-1/Al/175	0.080	0.12	207	62
ITH-2	0.125	0.005	313	28
ITH-2/Al/80	0.124	0.07	400	166
ITH-2/Al/175	0.101	0.17	275	90
ITH-6	0.138	0.13	321	68
ITH-6/Al/80	0.141	0.18	345	86
ITH-6/Al/175	0.130	0.13	303	64

[a] micropore volume and external surface area were evaluated from the t-plot method.

[b] evaluated using BJH method.

[c] surface area was evaluated using adsorption branch in the range p/p_s = 0.05 – 0.25

Both *ITH-6* zeolite and its aluminated derivatives *ITH-6/Al/80* and *ITH-6/Al/175* are characterized by high V_{meso} values, related to the adsorption of nitrogen in the interparticle space of the crystals (**Table 3**). Alumination of *ITH-1* and *ITH-2* zeolites decreased micropore volume but increased volume of mesopores, in the range of 0.3-0.8 of p/p_0 (**Table 3**). This corresponds to the formation of extra pores in the course of Ge extraction during alumination of *ITH-1* and *ITH-2* enhancing with increasing temperature of the treatment. The higher values of external surface area S_{ext} for *ITH-1/Al/80* and *ITH-2/Al/80* with respect to the initial germanosilicates (**Table 3**) agree with the results of SEM showing the decreasing average crystal size after alumination of Ge-rich **ITH** zeolites at 80 °C (**Fig. 2**).

3.2 The nature and concentration of acid sites

FTIR spectroscopy was used to investigate the evolution of OH-groups during alumination of **ITH** zeolites with different chemical compositions; the relevant spectra are depicted in **Fig. 5A**. Parent germanosilicates showed two absorption bands (at ca 3745 and 3633 – 3653 cm^{-1}) in the region 3800 – 3500 cm^{-1}. While the intensity of the band at 3745 cm^{-1} attributed to silanol groups increased with decreasing crystal size of germanosilicate **ITH** zeolites (*ITH-2* < *ITH-1* < *ITH-6* (**Fig. 5A, Table 1**), a broad absorption band at 3633 – 3653 cm^{-1} attributed to external Ge–OH groups[28] grew with increasing Ge content in the following sequence: *ITH-6* < *ITH-2* < *ITH-1*.

The increased absorption band at 3745 cm^{-1} in the spectra of *ITH-n/Al/80* zeolites with respect to parent germanosilicate indicates the formation of silanol defects under conditions used (**Fig. 5A**). In contrast, *ITH-n/Al/175* and *ITH-n* zeolites showed absorption bands at 3745 cm^{-1} of comparable intensities (**Fig. 4A**). This indicates the acceleration of Al incorporation into the framework of **ITH** zeolite accompanied with some healing of silanol defects with increasing temperature of the treatment. In agreement with this assumption, **ITH** zeolites aluminated at 175 °C are characterized by more intensive absorption band assigned to the bridging hydroxyl groups (cca. 3620 cm^{-1}, **Fig. 5A**) compared with the samples treated at 80 °C.

The incorporation of Al atoms into the framework of **ITH** zeolites in the course of the post-synthesis treatment was confirmed by FTIR spectroscopy of adsorbed pyridine. The appearance of the absorption band at 1545 cm^{-1} assigned to the pyridinium ion in the spectra of aluminated **ITH** zeolites clearly evidences the incorporation of aluminium into the framework positions [25] (**Fig. 5B**). In addition, alumination caused the increase in the intensity of the absorption band at 1455 cm^{-1}, which is obviously connected with increased concentration of Lewis acid centres [25] in aluminated **ITH** zeolites in comparison with initial germanosilicates.

The concentrations of Brønsted and Lewis acid sites determined from the integral intensities of the bands at 1545 and 1455 cm^{-1} using extinction coefficients[20] are given in **Table 4**. *ITH-6/Al/80* (c_B = 97; c_L = 194 μmol g^{-1}) and *ITH- 6/Al/175* (c_B = 239; c_L = 150 μmol g^{-1}) samples having the smallest crystals showed the highest concentrations of incorporated acid centres despite a relatively low concentration of hydrolytically unstable Ge–O(Si) bonds (**Table 1**). For zeolites of the comparable crystal size (e.g. *ITH-1*, *ITH-2*), the amount of incorporated acid centres increased with decreasing Si/Ge ratio in the parent germanosilicate.

Cite this: DOI: 10.1039/c0xx00000x

www.rsc.org/xxxxxx

ARTICLE TYPE

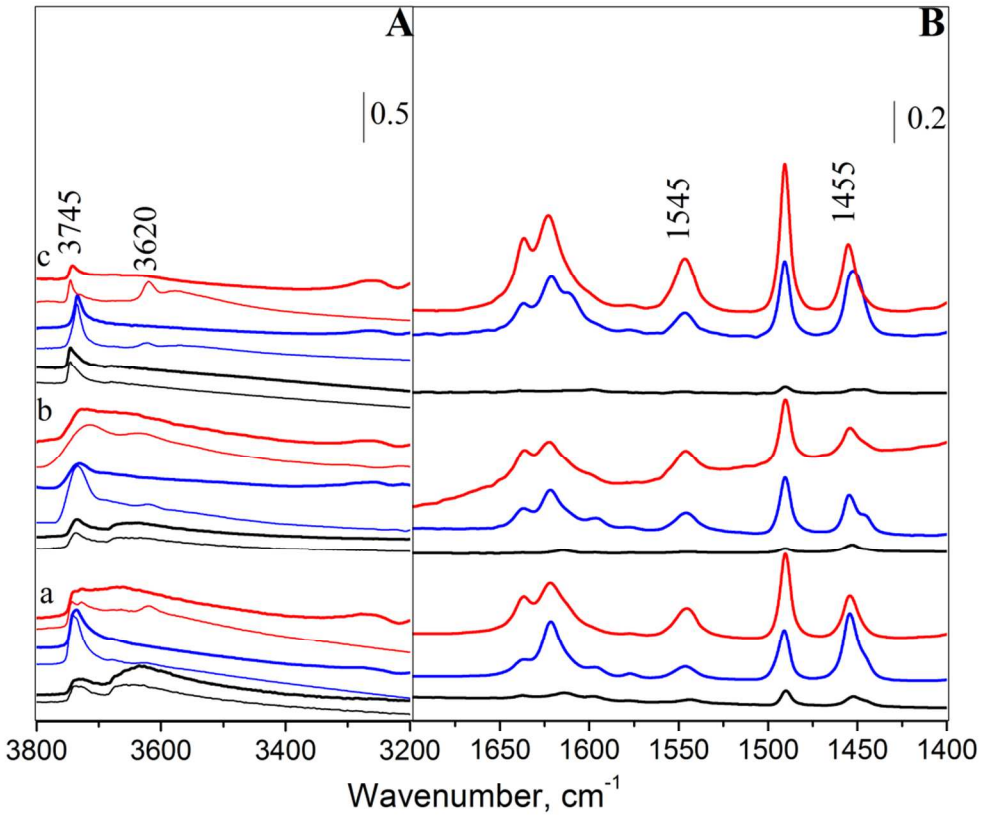

Fig. 5 IR spectra of *ITH-1* (**a**), *ITH-2* (**b**), *ITH-6* (**c**) zeolites (initial germanosilicates (black), *ITH-n/Al/80* (blue) and *ITH-n/Al/175* (red)): (A) region of hydroxyl vibrations; (B) region of pyridine vibrations. Down/thin lines show spectra before adsorption of pyridine, while top/bold show spectra after adsorption of base molecule

Table 4 The concentration of Lewis and Brønsted acid sites within **ITH** zeolites, determined by means of FTIR spectroscopy of adsorbed PY and DTBP

Sample	c_B μmol g^{-1}		c_L μmol g^{-1}	c_Σ μmol g^{-1}	Al_{FR}[a] μmol g^{-1}	c_Σ/Al_{FR}, %
	Pyridine	DTBP	Pyridine			
ITH-1	–	–	26	26	–	–
ITH-1/Al/80	60	24	140	200	381	53
ITH-1/Al/175	140	4	100	240	624	38
ITH-2	–	–	20	20	–	–
ITH-2/Al/80	90	21	67	157	216	72
ITH-2/Al/175	127	1	48	175	279	62
ITH-6	–	–	13	13	–	–
ITH-6/Al/80	97	10	194	291	371	78
ITH-6/Al/175	239	8	150	389	594	65

[a]calculated based on the results of chemical analysis and relative integral intensity of peak at 60 ppm in ^{27}Al NMR spectra

This may be connected with 1) increasing concentration of hydrolytically unstable Ge–O(Si) bonds being the source of defects in the second step condensing with aluminium ions forming acid centres; 2) increasing average size of pores developing in the course of hydrolysis of available Ge–O(Si) bonds facilitating the diffusion of aluminium ions to the formed defects. In this way, the alumination of *ITH-1* zeolite containing 28.6 mol.% of Ge (**Table 1**) generated higher amount of acid centres (200 – 240 μmol g^{-1}, **Table 4**) when compared with *ITH-2* (18.9 mol.% of Ge)-derived samples (127 – and 175 μmol g^{-1}, **Table 4**). Remarkably increased concentration of formed Brønsted acid centres (1.5 – 2.5 times) at slightly decreased amount of Lewis acid sites (**Table 3**) with increasing temperature of alumination of **ITH** zeolites from 80 to 175 °C should be noticed.

From the first sight, a successful incorporation of Al atoms into the framework of medium-pore **ITH** zeolite in the course of the post-synthesis treatment seems to contradict to literature results,[29, 30] thoroughly disproving aluminium incorporation in acidic medium to medium-pore boralites with inner void being inaccessible for bulky hydrated aluminium cations. However, these studies were focused only on (boro)silicate zeolites. The presence of hydrolytically unstable "domains" (i.e. D4R SBUs) in *ITH-1* and *ITH-2* zeolites seems to create the necessary prerequisites for incorporation of Al atoms. Since the conditions

Cite this: DOI: 10.1039/c0xx00000x

www.rsc.org/xxxxxx

ARTICLE TYPE

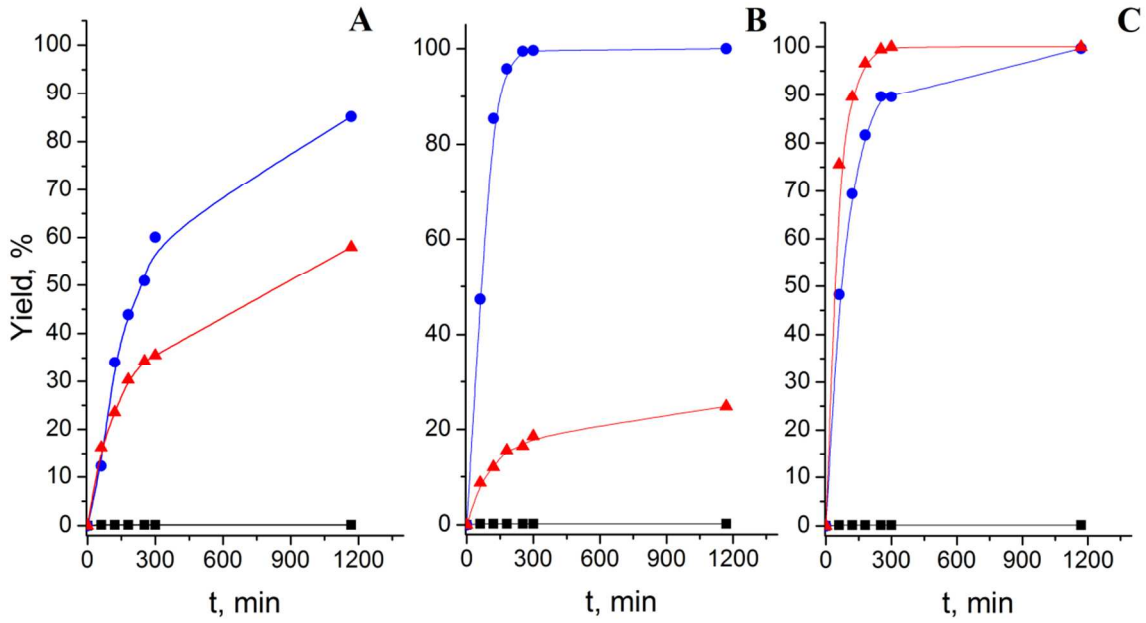

Fig. 6 Yield of tetrahydropyranyl ether versus time obtained in the reaction of methanol and DHP at 301 K over *ITH-1* (**A**), *ITH-2* (**B**), *ITH-6* (**C**)-derived zeolites: initial germanosilicates (black), *ITH-n/Al/80* (blue) and *ITH-n/Al/175* (red)

of the treatment (pH = 2.0, T = 80 or 175 °C) are sufficient for extraction of the most Ge from the framework (**Table 2**), it is reasonable to assume that the first stage of overall process is the breaking of Si–O–Ge bonds in D4Rs.[23] This leads to the formation of silanol defects in all **ITH** zeolites under investigation (**Fig. 5A**) as well as to the creation of ultramicro- and mesopores in *ITH-1* or *ITH-2* zeolites (**Fig. 4**). Thus, the development of extra-porosity in the course of *ITH-1* and *ITH-2* alumination seems to facilitate the penetration of hydrated aluminium cations in the inner volume of zeolite crystals followed by their condensation with Si-OH groups. At the same time, the "unsuitable" distribution of extractable Ge atoms in the framework (the absence of [4Si;4Ge] domains according to the NMR data [23]) in *ITH-6* zeolite seems to prevent the formation of extra-porosity (**Fig. 4C**). For the latter sample, 75% of Al forms intercrystalline extra-framework species with octahedrally coordinated aluminium (**Fig. 3**), whereas the formation of Brønsted acid sites (**Table 4**) likely proceeds mainly on the outer surface of the crystals.

Noticeably, the concentration of framework Al (Al_{FR}, **Table 4**) calculated based on the results of ^{27}Al NMR exceeds the total concentration of acid sites determined using Py as probe molecule. This is obviously connected with different accessibility of incorporated Al atoms being dependant on the treatment conditions and crystal size of aluminated **ITH** zeolites. Lower fraction of acid centres detectable for Py is characteristic for *ITH-n/Al/175* (38–62%, **Table 4**) vs. *ITH-n/Al/80* zeolites (53–78%, **Table 4**). This result may indicate the incorporation of a higher amount of Al to "inner" domains of **ITH** crystals with increasing the temperature of alumination. Remarkably higher concentrations of surface Brønsted acid centres for *ITH-1/Al/80* towards *ITH-1/Al/175* and similarly for *ITH-2*-derived samples (**Table 4**) were also detected using FTIR spectroscopy of adsorbed DTBP (the size of the DTBP molecule is about 7.9 Å,[21] which is higher than the diameter of 10-ring channels in zeolites). Higher accessibility of acid centres in *ITH-2*-derived samples (62; 72 %, **Table 4**) vs. *ITH-1* derivatives (38; 53 %, **Table 4**) is probably connected with larger fraction of mesopores within of *ITH-2/Al* vs. *ITH-1/Al* (**Table 3**). Naturally, *ITH-6/Al* zeolites characterized by tiny crystals (**Fig. 2**) showed the highest accessibility of acid centres (65 and 78 %, **Table 4**) among zeolites under investigation. According to the results of FTIR spectroscopy of adsorbed DTBP *ITH-6* zeolites aluminated at different temperatures insignificantly differ in the concentration of surface Brønsted acid sites detected with DTBP (8 – 10 μmol g^{-1}, **Table 4**).

3.3 Catalytic performance of Al-substituted ITH zeolites in tetrahydropyranylation of alcohols

The activity of various heterogeneous catalysts in the tetrahydropyranylation of alcohols may be attributed to both Brønsted and Lewis acid sites.[18, 31] The catalytic behavior of aluminated **ITH** zeolites was investigated in tetrahydropyranylation of methanol, 1-propanol and 1-hexanol.

While practically no conversion of substrates was observed over initial germanosilicate **ITH** zeolites possessing only a small

Cite this: DOI: 10.1039/c0xx00000x

www.rsc.org/xxxxxx

ARTICLE TYPE

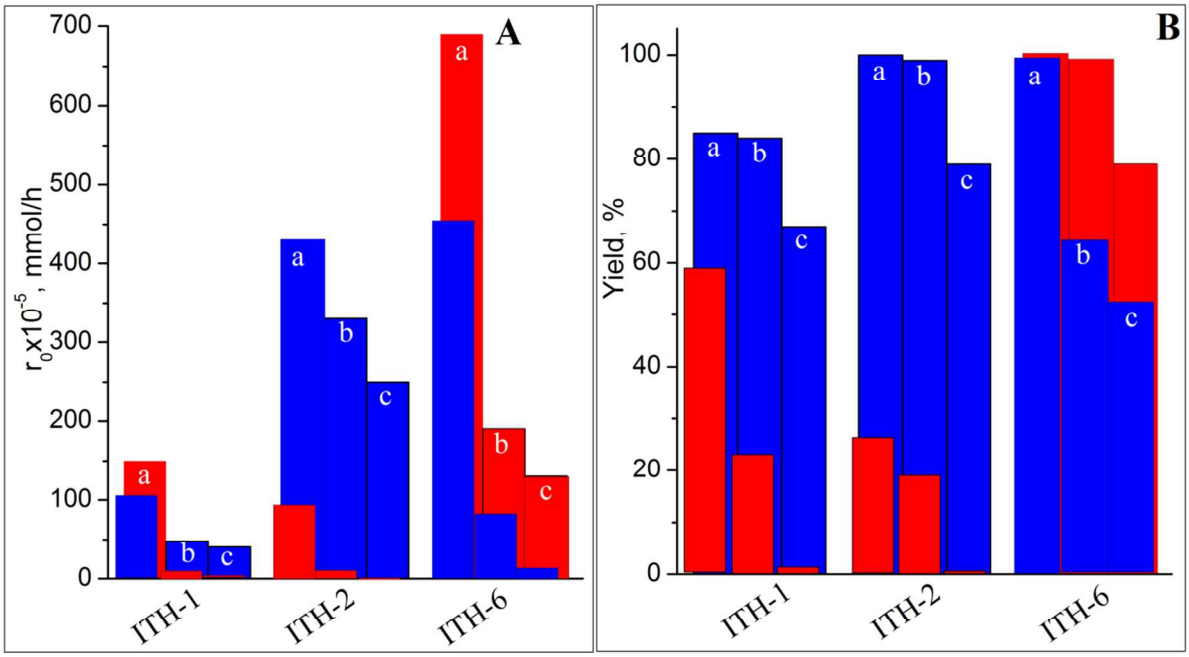

Fig. 7 Initial rate (**A**) and the yield of tetrahydropyranyl ethers (**B**) formed in the reaction of methanol (a), 1-propanol (b) and 1-hexanol (c) over **ITH** zeolites aluminated at 80 °C ( ) and at 175 °C ( )

amount of weak Lewis acid centres (**Fig. 6**, **Table 4**), the only products of alcohols transformation formed in reaction mixture over Al-containing zeolites under investigation were targeted tetrahydropyranyl ethers (**Scheme 1**). Relative amount of dimer formed in the competitive bimolecular dimerization of DHP did not exceed 6 mol.%.

The yield of tetrahydropyranyl ether obtained in the reaction of methanol and DHP after 1200 min was found to increase in the following order of catalysts: *ITH-2/Al/175* (25%) < *ITH-1/Al/175* (58%) < *ITH-1/Al/80* (85%) < *ITH-6/Al/80* (100%) = *ITH-6/Al/175* (100%) = *ITH-2/Al/80* (100%) (**Fig. 6**). Noticeably, *ITH-n/Al/80* (n = 1; 2) samples characterizing by higher accessibility of acid sites performed better than *ITH-n/Al/175* (n = 1; 2) zeolites. In particular, *ITH-2/Al/175* possessing higher concentration of acid centres than *ITH-2/Al/80* (175 vs. 157 μmol/g, **Table 3**) showed remarkably lower initial rate in methanol tetrahydropyranylation ($80 \cdot 10^{-5}$ vs. $430 \cdot 10^{-5}$ mmol·h^{-1}, **Fig. 7**). At the same time, while *ITH-1/Al/80* (S_{ext} = 143 m^2 g^{-1}, **Table 3**) and *ITH-1/Al/175* (S_{ext} = 62 m^2 g^{-1}, **Table 3**) were characterized by similar initial reaction rates in methanol transformation ($110 - 150 \cdot 10^{-5}$ mmol·h^{-1}, **Fig. 7A**), *ITH-1/Al/80* with a larger S_{ext} (accessibility of acid sites) showed a higher yield of target ether (**Fig. 7B**). The obtained results may indicate that diffusion constraints exist in prepared micro/mesoporous **ITH** zeolites possessing big crystals (i.e. *ITH-1* and *ITH-2* aluminated derivatives) even when using methanol as a substrate.

Diffusion limitations seem not to play so decisive role in tetrahydropyranylation of methanol over aluminated *ITH-6* zeolites having the smallest crystals of 5.0 x 0.5 x 0.5 μm (**Table 1, Fig. 2H, I**). In this way, *ITH-6/Al/80* (S_{ext} = 86 m^2 g^{-1}, **Table 2**) showed 4-times higher initial rate in methanol tetrahydropyranylation (**Fig. 7A**) in comparison with *ITH-1/Al/80* (S_{ext} = 143 m^2 g^{-1}, **Table 2**) (**Fig. 7A**). A superior performance of *ITH-6/Al/80* having higher total concentration of acid sites (291 vs. 200 μmol g^{-1}, **Table 3**) in transformation of methanol can be explained taking into account the possibility of substrate activation by "inner" acid centres. In contrast, *ITH-1/Al/80* (67 – 84% yield, **Fig. 7B**) performed better than *ITH-6/Al/80* (52 – 64% yield, **Fig. 7B**) when using bulkier 1-propanol and especially 1-hexanol as substrate. This result is likely connected with the increasing role of external acid sites in the activation of bulky alcohols.

A decrease in the activity of all aluminated **ITH** samples (**Fig. 7**) was observed when the size of the reactants increased (methanol (kinetic diameter 3.6 Å) < 1-propanol (4.7 Å) < 1-hexanol (6.2 Å).[32] Again, *ITH-1/Al/80* and *ITH-2/Al/80* showed higher initial rates of alcohol transformation (**Fig. 7A**) and yields of target ethers (**Fig. 7B**) vs. *ITH-1/Al/175* and *ITH-2/Al/175* possessing lower S_{ext} (accessibility of acid sites). It should be noted, that particular results of DTBP (a selective probe molecule for Brønsted sites[33]) adsorption and activity of prepared *ITH-n/Al* samples in tetrahydropyranylation of alcohols can hardly be

correlated without considering total concentration of accessible acid sites (both Brønsted and Lewis) formed on the external surface. In particular, comparing *ITH-1/Al/80* (S_{ext} = 143 m^2 g^{-1}, **Table 2**) and *ITH-2/Al/80* (S_{ext} = 166 m^2 g^{-1}, **Table 2**), a very similar amount of external Brønsted acid sites (**Table 3**) gives massively different activities (**Fig. 7**), which may be related to the higher S_{ext} of more active *ITH-2/Al/80*. On the other hand, catalytic activity of prepared Al-substituted **ITH** zeolites cannot be correlated only with their textural characteristics. For instance, *ITH-1/Al/175* (S_{ext} = 62 m^2 g^{-1}, **Table 2**) showed higher yields, despite having lower S_{ext} than *ITH-2/Al/175* (S_{ext} = 90 m^2 g^{-1}, **Table 2**). This agrees with higher concentration of surface Brønsted acid sites in *ITH-1/Al/175* (**Table 3**).

In contrast, total acidity likely determines the catalytic behavior of *ITH-6* aluminated derivatives when using 1-propanol and 1-hexanol as substrates. *ITH-6/Al/80* possessing lower total number of acid sites (c_{Σ} = 292 μmol g^{-1}) shows lower initial rates and yields in tetrahydropyranylation of 1-propanol and 1-hexanol than *ITH-6/Al/175* (c_{Σ} = 391 μmol g^{-1}) (**Fig. 7**) despite having similar number of external Brønsted acid sites (**Table 3**) and higher S_{ext} (**Table 2**). This result can be rationalized considering lower pass length of reacting molecules into and off tiny crystals of Al-containing *ITH-6* zeolites and assuming activation of substrate molecules (kinetic diameters < 6.2 Å) with acid centres inaccessible for DTBP (kinetic diameter = 7.9 Å) within *ITH-6/Al* catalysts.

ITH-2/Al/80 zeolite possessing highest value of S_{ext} (166 m^2 g^{-1}, **Table 2**) showed the highest initial rates when using 1-propanol ($r_0 = 330 \cdot 10^{-5}$ mmol·h^{-1}) and 1-hexanol ($r_0 = 250 \cdot 10^{-5}$ mmol·h^{-1}) as substrates (**Fig. 7**). However, it should be noted, that the yields achieved over *ITH-2/Al/80* possessing relatively high S_{ext} and *ITH-6/Al/175* having the highest concentration of acid sites are comparable (**Fig. 7**). This agrees with higher concentration of acid centres activating substrate molecules in initial time within ITH-2/Al/80 (e.g. surface acid centres), while involving of "inner" acid sites of *ITH-6/Al/175* in catalytic process in time.

4. Conclusions

Alumination of Ge-rich medium-pore **ITH** zeolites (Si/Ge = 2.5 and 4.4) in acidic medium (pH = 2) was found to result not only in the formation of strong Brønsted and Lewis acid sites, but also in the development of extra porosity, related to the extraction of Ge off D4Rs SBUs regularly arranged in initial germanosilicates. In contrast, no extra-porosity was formed in the course of alumination of Ge-poor **ITH** zeolite (Si/Ge = 5.8).

The chemical composition and crystal size of initial zeolite as well as the temperature of post-synthesis treatment was shown to determine the total concentration and accessibility of formed acid centres as well as the ratio between Brønsted and Lewis acid sites.

For Ge-rich **ITH** zeolites showing bulky crystals (e.g. 10.0 x 2.5 x 1.0 μm) the amount of incorporated acid centres increased with decreasing Si/Ge ratio in the parent germanosilicate, which is likely connected with 1) increased concentration of hydrolytically unstable Ge–O(Si) bonds being the source of defects further condensed with aluminium ions forming acid centres; 2) increased average size of pores developed during hydrolysis of available Ge–O(Si) bonds, which facilitate the diffusion of aluminium ions to the formed defects. Ge-poor **ITH** zeolite possessing the smallest crystals (i.e. 5.0 x 0.5 x 0.5 μm) showed the highest concentration of incorporated acid centres (291 and 389 μmol g^{-1} for the samples aluminated at 80 and 175 °C, respectively).

The formation of larger pores at 175 °C enhanced the diffusion of Al species as well as acceleration of the rates of condensation reactions leading to the formation of Si–O–Al bonds. This led to the remarkable increase (1.5 – 2.5 times) in the concentration of formed Brønsted acid centres at slightly decreased amount of Lewis acid sites in aluminated **ITH** zeolites independently on the chemical composition of parent germanosilicate.

In contrast to alumination at 80 °C, the treatment of germanosilicate **ITH** zeolites at 175 °C was accompanied with decreasing fraction of framework Al atoms detectable with base probe molecules (i.e. pyridine, 2,6-di-*tert*-butyl-pyridine), i.e. the increased concentration of the "inner" acid sites.

The activity of prepared Al-substituted **ITH** zeolites possessing big crystals (e.g. 10.0 x 2.5 x 1.0 μm) was found not depending on the total concentration of acid centres, indicating diffusion constraints existing in prepared micro/mesoporous **ITH** zeolites even when using methanol as a substrate in tetrahydropyranylation reaction. In general, Ge-rich **ITH** zeolites (Si/Ge = 2.5 and 4.4) aluminated at 80 °C having higher S_{ext} and concentration of accessible acid sites performed better in tetrahydropyranylation of alcohols than samples aluminated at 175 °C. In contrast, activity of aluminated derivatives of Ge-poor **ITH** zeolite (Si/Ge = 5.8) possessing tiny crystals (i.e. 5.0 x 0.5 x 0.5 μm) increased with growth of the total concentration of acid centres. A decrease in the activity of all aluminated **ITH** samples was observed when the size of the reactants increased (methanol (kinetic diameter 3.6 Å) < 1-propanol (4.7 Å) < 1-hexanol (6.2 Å).

5. Acknowledgements

Authors thank Dr. Daniel Dawson (University of St Andrews) for the providing of NMR data. M.S. thanks the Czech Science Foundation for the support of the Project 14-30898P, M.O. acknowledges the Czech Science Foundation for the Project 13-17593P. R.E.M thanks the EPSRC for funding (EP/K025112/1 and EP/L014475/1).

6. Notes and references

[a] *J. Heyrovský Institute of Physical Chemistry of the Czech Academy of Sciences, v. v. i., Dolejškova 3, CZ-182 23 Prague 8, Czech Republic. Fax: (+420)286 582 307; Tel: (+420)266053795; E-mail: jiri.cejka@jh-inst.cas.cz*

[b] *L.V. Pisarzhevskiy Institute of Physical Chemistry, National Academy of Sciences of Ukraine, pr. Nauky, 31 Kyiv 03028, Ukraine. Fax: (+380)445 256 216; Tel: (+380)445 254 196*

[c] *Micro and Mesoporous Molecular Sieves Group, Institute of Chemistry, University of Campinas, Rua Monteiro Lobato, 270, 13083-861, Cidade Universitária Zeferino Vaz, Campinas, SP, Brazil.*

[d] *EaStCHEM School of Chemistry, University of St. Andrews, St. Andrews KY16 9ST, United Kingdom.*

1. D. Kubicka, I. Kubickova and J. Čejka, *Catal. Rev. Sci. Eng.*, 2013, **55**, 1-78.
2. S. M. Csicsery, in *Stud. Surf. Sci. Catal.*, eds. H. K. Beyer, H. G. Karge, I. Kiricsi and J. B. Nagy, 1995, vol. 94, pp. 1-12.
3. W. J. Roth, P. Nachtigall, R. E. Morris, P. S. Wheatley, V. R. Seymour, S. E. Ashbrook, P. Chlubna, L. Grajciar, M. Polozij, A. Zukal, O. Shvets and J. Čejka, *Nat. Chem.*, 2013, **5**, 628-633.
4. P. S. Wheatley, P. Chlubná-Eliášová, H. Greer, W. Zhou, V. R. Seymour, D. M. Dawson, S. E. Ashbrook, A. B. Pinar, L. B. McCusker, M. Opanasenko, J. Čejka and R. E. Morris, *Angew. Chem. Int. Ed.*, 2014, **53**, 13210-13214.
5. A. Corma, M. J. Diaz-Cabanas, J. L. Jorda, F. Rey, G. Sastre and K. G. Strohmaier, *J. Am. Chem. Soc.*, 2008, **130**, 16482-16483.
6. M. Kubů, S. Zones and J. Čejka, *Top. Catal.*, 2010, **53**, 1330-1339.
7. S. Smeets, D. Xie, L. B. McCusker, C. Baerlocher, S. I. Zones, J. A. Thompson, H. S. Lacheen and H.-M. Huang, *Chem. Mater.*, 2014, **26**, 3909-3913.
8. J. Čejka, A. Vondrová, B. Wichterlová, G. Vorbeck and R. Fricke, *Zeolites*, 1994, **14**, 147-153.
9. A. Corma, M. Puche, F. Rey, G. Sankar and S. J. Teat, *Angew. Chem. Int. Ed.*, 2003, **42**, 1156-1159.
10. T. Boix, M. Puche, M. A. Camblor and A. Corma, *Synthetic porous crystalline material ITQ-13 its synthesis and use*, US 6,471,941
11. M. V. Shamzhy, O. V. Shvets, M. V. Opanasenko, P. S. Yaremov, L. G. Sarkisyan, P. Chlubna, A. Zukal, V. R. Marthala, M. Hartmann and J. Cejka, *J. Mater. Chem.*, 2012, **22**, 15793-15803.
12. O. V. Shvets, M. V. Shamzhy, P. S. Yaremov, Z. Musilova, D. Prochazkova and J. Čejka, *Chem. Mater.*, 2011, **23**, 2573-2585.
13. R. Castaneda, A. Corma, V. Fornes, J. Martinez-Triguero and S. Valencia, *J. Catal.*, 2006, **238**, 79-87.
14. J. S. Buchanan, J. M. Dakka, X. Feng and J. G. Santiesteban, *Aromatics conversion with ITQ-13*, US7081556 B2
15. J. A. Vidal-Moya, T. Blasco, F. Rey, A. Corma and M. Puche, *Chem. Mater.*, 2003, **15**, 3961-3963.
16. X. Ren, J. Liu, Y. Li, J. Yu and R. Xu, *J. Porous Mater.*, 2013, **20**, 975-981.
17. M. Shamzhy and F. S. d. O. Ramos, *Catal. Today*, 2015, **243**, 76-84.
18. G. Sartori, R. Ballini, F. Bigi, G. Bosica, R. Maggi and P. Righi, *Chem. Rev.*, 2003, **104**, 199-250.
19. G. Sastre, A. Pulido, R. Castañeda and A. Corma, *J. Phys. Chem. B*, 2004, **108**, 8830-8835.
20. C. A. Emeis, *J. Catal.*, 1993, **141**, 347-354.
21. M. A. Camblor, A. Corma, H. García, V. Semmer-Herlédan and S. Valencia, *J. Catal.*, 1998, **177**, 267-272.
22. C. Baerlocher, L. B. McCusker and D. H. Olson, *Atlas of zeolite framework types*, Elsevier, Amsterdam, 2007.
23. M. Shamzhy, M. Opanasenko, Y. Tian, K. Konysheva, O. Shvets, R. E. Morris and J. Čejka, *Chem. Mater.*, 2014, **26**, 5789-5798.
24. R. Dutartre, L. C. de Ménorval, F. Di Renzo, D. McQueen, F. Fajula and P. Schulz, *Micropor. Mater.*, 1996, **6**, 311-320.
25. J. C. Groen, L. A. A. Peffer, J. A. Moulijn and J. Pérez-Ramírez, in *Stud. Surf. Sci. Catal.*, eds. S. Abdelhamid and J. Mietek, Elsevier, 2005, vol. 156, pp. 401-408.
26. in *Multinuclear Solid-State NMR of Inorganic Materials*, eds. J. D. M. Kenneth and E. S. Mark, Pergamon, 2002, vol. 6, pp. 271-330.
27. L. Burel, N. Kasian and A. Tuel, *Angew. Chem. Int. Ed.*, 2014, **53**, 1360-1363.
28. M. Moliner, M. J. Díaz-Cabañas, V. Fornés, C. Martínez and A. Corma, *J. Catal.*, 2008, **254**, 101-109.
29. C. Y. Chen and S. I. Zones, *Method for heteroatom lattice substitution in large and extra-large pore borosilicate zeolites*, US 6,468,501
30. C.-Y. Chen and S. I. Zones, in *Zeolites and Catalysis*, Wiley-VCH Verlag GmbH & Co. KGaA, 2010, pp. 155-170.
31. P. G. M. Wuts and T. W. Greene, in *Greene's Protective Groups in Organic Synthesis*, John Wiley & Sons, Inc., 2006, pp. 431-532.
32. H. Wu, Q. Gong, D. H. Olson and J. Li, *Chem. Rev.*, 2012, **112**, 836-868.
33. K. Góra-Marek, K. Tarach and M. Choi, *J. Phys. Chem. C*, 2014, **118**, 12266-12274.